Design and construction of the X-ray instrumentation onboard the *HaloSat* CubeSat

Daniel M. LaRocca[a*], Philip Kaaret[a], Donald L. Kirchner[a], Anna Zajczyk[a,b,c], William Robison[a], Thomas E. Johnson[b], Keith M. Jahoda[b], William Fuelberth[a], Hannah C. Gulick[a], Ross McCurdy[a], Keith White[a], Drew M. Miles[a]

[a]University of Iowa, Kaaret Research Group, Department of Physics and Astronomy, 30 N Dubuque St., Iowa City, IA, USA, 52240

[b]NASA Goddard Space Flight Center, Greenbelt, MD, USA, 20771

[c]University of Maryland, Baltimore County, Department of Physics, 1000 Hilltop Circle, Baltimore, MD, USA, 21250

Abstract. *HaloSat* is the first mission funded by NASA's Astrophysics Division to use the CubeSat platform. Using three co-aligned silicon drift detectors, the *HaloSat* observatory measures soft (0.4-7 keV) X-ray emission from sources of diffuse emission such as the hot, gaseous halo of the Milky Way. In this paper, we describe the design and construction of the science payload on *HaloSat* and the reasoning behind many of the choices. As a direct result of the design choices and adherence to best practices during construction, the *HaloSat* science payload continues to perform well after more than one year on-orbit.

Keywords: CubeSat, X-ray, Instrumentation, Astronomy, Halo.

*Daniel M. LaRocca, daniel-larocca@uiowa.edu

1 Introduction

CubeSats are housed in canisterized satellite dispensers (CSDs), which increase launch flexibility and opportunity by isolating payloads from their launch vehicles [1]. The modest cost and rapid timescales on which CubeSats can be developed make them an intriguing prospect for getting hardware into space. Initially, the CubeSat program was an educational tool to familiarize students with the process of launching and operating small satellites [2]. Since then, the CubeSat platform has gained popularity, with over 200 of the form factor 3U and 14 6U released in 2017 [3]. CubeSats have served as technology demonstrations and for complementing the objectives of larger missions. As they have grown larger and more reliable, CubeSats also serve as a low-cost option for research in space and have become capable of conducting specialized missions.

Research in X-ray astrophysics stands to benefit from the widespread use of CubeSats. X-ray

emission is entirely blocked by the atmosphere, preventing ground-based X-ray observations and serving as a barrier for smaller missions. While many CubeSats conduct heliophysics or Earth imaging, few have been used for astrophysical pursuits. *HaloSat* is the first mission funded by NASA's Astrophysics Division to use the CubeSat form factor. *HaloSat* was designed to measure the diffuse X-ray emission from the hot, gaseous halo of the Milky Way to constrain its estimated mass and geometry [4]. Before *HaloSat*, X-ray observations of halo emission did not cover the entire sky or were taken with poor spectral resolution. In comparison, the observations that have been made with *HaloSat* cover the whole sky with moderate spectral resolution (ΔE$<$80 eV) near the prominent oxygen emission features from the halo. These observations are conducted using a strategy that minimizes foreground contaminating emission from solar wind charge exchange [5]. *HaloSat* is a 12.0 kg CubeSat using the 6U form factor (10.5 cm$\times$22.5 cm$\times$36.5 cm) [6]. The science payload aboard *HaloSat* includes three redundant and co-aligned silicon drift detectors (SDDs) used to measure X-ray emission between 0.4-7 keV. *HaloSat* has the potential to answer scientifically lucrative questions at a relatively low cost.

While academic institutions remain a driving force in CubeSat development, a commercial sector dedicated to developing and supporting the numerous CubeSat missions has emerged [7]. The science payload aboard *HaloSat* was designed, constructed, and tested at the University of Iowa (UI); whereas its high-performance 6U spacecraft bus was built and operated by Blue Canyon Technologies (BCT). The 6U CubeSat bus provides a viable alternative to constructing an entirely customized bus, while adhering to the budgetary and time constraints required for the mission. The use of a commercial spacecraft bus also allowed for a UI science team with minimal previous experience in CubeSats to focus on the science payload development.

Funding for *HaloSat* began in January 2016 with a total budget of less than \$4M [4]. The

instrument was integrated with the spacecraft bus in October 2017, stowed in a NanoRacks CSD in March 2018, launched aboard the Orbital ATK Cygnus 9 commercial resupply to the International Space Station (ISS) in May 2018, and deployed in July 2018. Due to its 400km low-Earth orbit, *HaloSat* has an expected orbital lifetime of 26 months. Nominal operations began in October 2018 and are ongoing with BCT serving as the Mission Operations Center (MOC). BCT is conducting ground communication through collaboration with the Wallops Flight Facility Ground Station. The UI team serves as the Science Operations Center for observation planning and data reduction. Separating the science from mission operations leverages the expertise and specialization of the commercial and academic institutions in their respective roles.

In this paper, we focus on the design and construction of the science payload onboard *HaloSat*. We discuss a general overview of the science payload in Sec. 2, the mechanical layout in Sec. 3, the detector assembly in Sec. 4, the signal processing electronics in Sec. 5, the interface and control electronics in Sec. 6, and the payload software in Sec. 7.

2 Science Payload Overview

The science payload onboard *HaloSat* is the X-ray observing instrument built by the UI team. While the spacecraft bus provides power, attitude control, and communications, the science payload conducts the relevant science measurements and data collection. A 3D parts and assembly model as well as an image of the science payload can be seen in Fig. 1.

To accomplish the science objectives, the science payload must i) reliably detect X-ray emission between 0.4-2 keV, ii) have sufficient energy resolution to measure the sum of oxygen emission lines ($<$100 eV resolution), iii) have an angular resolution $<15^{\circ}$, but large enough to observe the entirety of the sky during the mission life, iv) reach a statistical accuracy of 10% for oxygen

line emission for sufficiently bright fields, and v) maintain background systematics below 10%.

Broadly categorized, the components of the instrument are the detector assembly, the signal processing electronics, and the interface and control electronics. The detector assembly converts each X-ray event into a charge pulse and shapes and amplifies that pulse. The signal processing electronics digitizes each pulse that surpasses threshold criteria. The interface and control electronics communicates with the spacecraft, receives and executes commands, sets threshold levels, and maintains detector temperature. It also encodes and packetizes science and housekeeping data for transfer to the spacecraft non-volatile storage and eventual downlink. The interface and control electronics also provides electromagnetic interference (EMI) filtering for spacecraft voltages and regulates voltages needed for the detector electronics.

Together, these systems comprise a single detector unit. The science payload system design has three block redundant detector units, each with independent signal and power interfaces to the spacecraft. The lack of shared electronics and electrical connections between the individual detector units allows each to operate independently and reduces the susceptibility to single point failures. The number of detector units was primarily constrained by the number of detector units that would physically fit in the available volume. Each unit provides additional collecting area, increasing the number of X-rays detected. The science payload has no focusing optics or imaging capabilities.

HaloSat is classified under NPR 7120.8 Research and Technology Development Programs and Projects, and as such is not subject to the NASA Policy Directive (NPD) 8730.2C NASA Parts Policy. To reduce cost, it is common for CubeSat payloads to not use radiation hardened electronic components. Components used complied with grade 4 as described in NASA-STD-8739.10 Electrical, Electronic, and Electromechanical (EEE) Parts Assurance Standard. Automotive grade

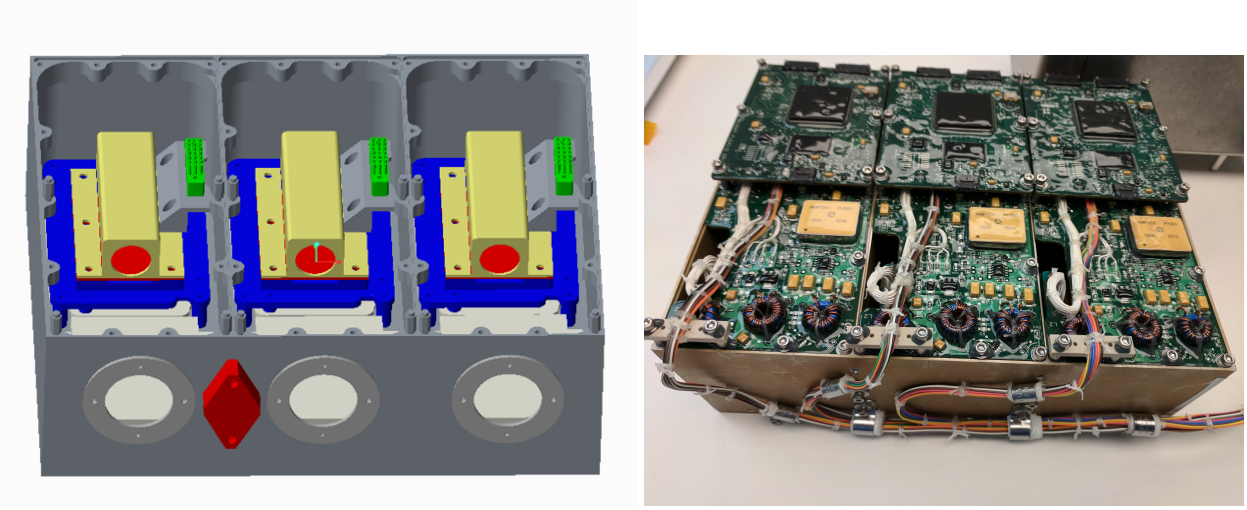

Fig 1 The *HaloSat* science payload is completely contained in a single aluminum sub-assembly. This sub-assembly is mounted inside the payload enclosure of the spacecraft bus. (Left) A 3D model of the science payload onboard the *HaloSat* observatory without the control and interface electronics. Each of the three compartments contains a detector assembly. (Right) A picture of the science payload viewed from behind prior to integration. The Analog printed circuit boards (PCBs) enclose the detector compartments and the digital processing unit PCBs are mounted.

commercial components were used, which has been successful for past CubeSat missions.

3 Mechanical Layout

The central structure of the science payload is 21.99 cm×16.80 cm×7.21 cm and is referred to as the instrument housing, which can be seen as the grey structure in Fig. 1. The instrument housing was milled from a single piece of 6061-T651 aluminum in the UI Department of Physics and Astronomy Machine Shop. The use of a single subassembly allowed the science payload to be a stand-alone device with no substantial rearranging required to conduct environmental testing (see Fig. 2). This is a practice to improve performance during vibration and thermal cycling in comparison to a series of disjointed sub-assemblies. A single structure also made assembly of the instrument straightforward and detector alignment could be measured for the entire instrument and translated to the spacecraft coordinate system. Furthermore, the science payload was integrated into the spacecraft bus without adjustments after testing.

The instrument housing has three compartments, each of which contains a detector unit. Mounted at the rear of each compartment is a detector assembly, consisting of the aluminum baseplate, the SDD, a passive radiation shield, and the detector front-end electronics. Each unit was tested and characterized independently and could be swapped with an available flight spare in the event of an anomaly.

The integral thermoelectric cooler (TEC) in each SDD generates heat during operation, therefore the SDD package must be in thermal contact with a surface capable of dissipating this heat. Each SDD is fastened to a 17 mm tall and 3 mm thick aluminum protrusion extending from the detector assembly baseplate (referred to as the "tombstone"). Because the tombstone and baseplate are fabricated from a single block of aluminum, the SDD is in good thermal contact with the detector assembly baseplate with no intervening bolted interface. The baseplate is tightly thermally coupled to the instrument housing, creating a thermal path for dissipating heat. The SDD mounting stud and 12 insulated pins pass through holes in the tombstone. The stud was fastened using a nut and lock washer torqued to 0.79 $\mathrm{N} \cdot \mathrm{m}$. The detector assembly baseplate has a 14.5 mm$\times$29.0 mm surface in contact with the instrument housing using four fasteners to ensure adequate thermal contact.

The detector front-end electronics are housed on a four-layer 63 mm$\times$87 mm printed circuit board (PCB) mounted to the underside of the detector assembly and referred to as the Amp-Chain PCB. For the interface to the SDD, wires were lap soldered to the Amp-Chain PCB, extended through an opening in the baseplate, routed along the tombstone, and directly soldered to the pins of the SDD. Significant consideration was given to the thermal environment expected for a CubeSat. The small mass and short orbit duration for *HaloSat* required that the instrument withstand a large number of thermal cycles over the mission life. Direct solder joints were chosen over a more

traditional plug board concept due to concerns of the impact that thermal cycling might have on the non-soldered connections. The solder joints allowed for the lacing and staking of the wire bundle to the tombstone with service loops to reduce stress from thermal expansion experienced by the pins of the SDD. The entire connection interface was potted using room temperature vulcanizing silicone. This potting encapsulated the SDD pins and the central stud to prevent shorts and reduce stress on the pins.

Each SDD is mounted inside of a passive radiation shield consisting of a plate and a box (see Fig. 3). The plate is a 1.4 mm thick 51.0 mm$\times$42.5 mm sheet fastened to the baseplate just below the SDD at the base of the tombstone. The box is 1.2 mm thick with dimensions 65.0 mm$\times$22.5 mm$\times$20.0 mm and surrounds the detector. The passive shield must not obstruct any X-rays passing through the aperture to the detector, hence the side of the box between the detector and the X-ray aperture has a 15.85 mm diameter circular opening. The angular size of the passive shield opening viewed from the SDD is larger than the angular size of the field of view (FOV) of the detectors. There is a second unshielded 15.0 mm$\times$8.3 mm opening behind the tombstone for the wires connecting the SDD to the front-end electronics.

Each SDD detects X-rays from astrophysical sources through a geometric X-ray collimator determined by the inner diameter of a 0.78 mm thick circular aluminum alignment washer. The alignment washers are fastened to the instrument housing and form the X-ray aperture through which the detectors observe the sky. The attenuation of the X-ray radiation through the washer vignettes the signal, which restricts and co-aligns the FOV. The washers were designed to produce a FOV with a full-response radius of 5° and a zero-response radius of 7°. The alignment of the individual detectors is accurate to within $\pm$0.23° of an averaged central payload boresight vector [4]. Had the alignment notably differed between units, replacement washers would have been

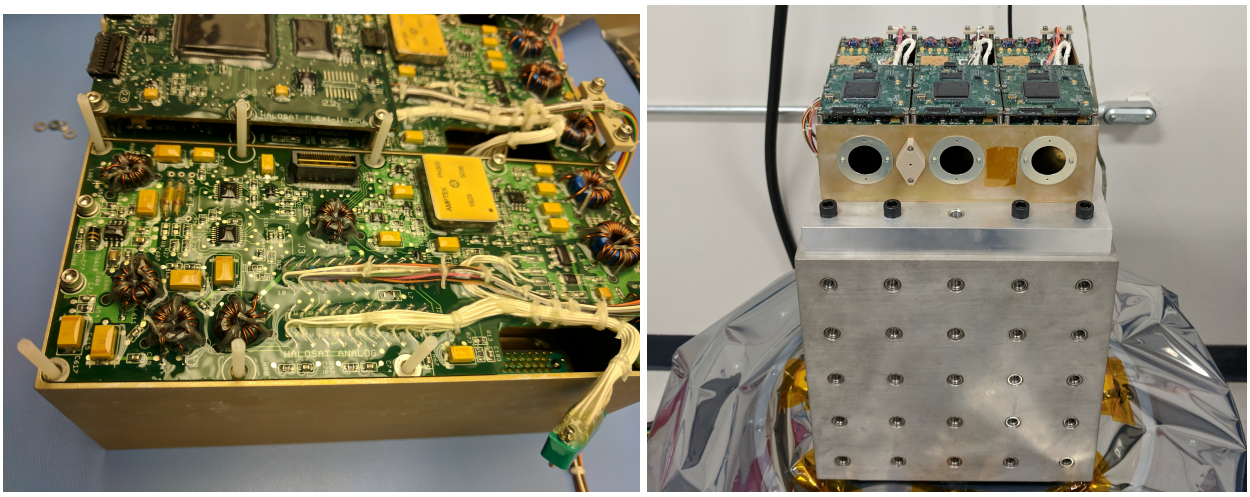

Fig 2 (Left) An image of the instrument as the final Analog PCB was mounted. The green MIL-DTL-28478 and its mate can be seen. The Samtec connection interface to the DPU is also visible. (Right) The instrument was fully assembled in flight configuration for vibration testing at Wallops Flight Facility. The single sub assembly allowed testing and integration to progress smoothly. The aluminum alignment washers are attached. The mirror cover can be seen between the first and second apertures from the left.

fabricated to ensure detector agreement.

To provide a reference vector for measuring the boresight for each of the detectors and translating the payload coordinates into the spacecraft coordinate system, the normal vector relative to a flat mirror was measured in both coordinate systems. This mirror adheres to the surface of the instrument housing between the first and second X-ray apertures. A mirror cover was installed following the completion of alignment measurements to protect the spacecraft from possible mirror fragments.

Use of a cylindrical X-ray collimator was considered, but not implemented due to conflicting structure with the detector shielding. During construction, an examination of ray tracing models also suggested that in the designed configuration, internal reflections from a cylindrical collimator would add more contamination than a single washer aperture.

For each detector unit, a 67 mm$\times$69 mm PCB houses a high voltage power supply (HVPS) and is mounted in the compartment between the detector assembly and the apertures, but outside of the

observing FOV. The HVPS output interfaces directly to the Amp-Chain PCB. The input power and control interface to the Analog PCB uses a MIL-DTL-28478 connector discussed below.

For each detector unit, a six-layer 71.3 mm$\times$167.5 mm Analog PCB is mounted directly on the instrument housing and encloses the detector assembly compartment. A ground layer in the Analog PCB electrically contacts the lip of the instrument housing to create a Faraday cage to shield the detector. All digital signals were kept outside of the compartment to reduce the electronic noise injected before amplification, therefore all signals in the compartment are analog. The Analog PCB interfaces with the Amp-Chain PCB and the HVPS through the MIL-DTL-28478 connector mounted on the detector assembly with an aluminum bracket. There is also an AC connection between the Analog PCB electrical ground and the instrument housing provided by four 0.1 μF capacitors. Several capacitor configurations were evaluated while connected to an engineering model of the spacecraft avionics, or engineering design unit (EDU), to determine which configuration gave the lowest noise on the detector readout.

Each detector unit has a six-layer 71.3 mm$\times$90.0 mm digital processing unit (DPU) PCB, mounted on six 8-mm stand-offs above the Analog PCB. An image of the Analog PCB taken just before mounting the final DPU PCB can be seen in Fig. 2. The DPU PCB contains a field-programmable gate array (FPGA) and the crystal oscillator. It interfaces to its Analog PCB using mating Samtec connectors (QTH-030-01-L-D-A/QSH-030-01-L-D-A). The individual detector units are identified from serialized resistors encoded on their DPUs, which are 14, 54, and 38 as viewed from left to right in Fig. 1 (left panel).

In total, the mass of the instrument is 2.78 kg. The instrument mechanically interfaces to the spacecraft using two alignment pins and slots. Slots were machined into the instrument housing to allow a slip fit depth of 9.5 mm for a 5 mm locating pin and 37 2D 4-40 helicoil inserts for fastening

to the spacecraft. There are three electrical interfaces for power and communications, one for each of the three detector units. This interface consists of a 15-pin MDM connector from the science payload (Glenair part M83513/04-B02N) to the spacecraft (Glenair part M83513/28-B01NN). The maximum average power dissipated by the instrument is 4.02 W with all three detectors in operation.

Printed wiring board (PWB) material was a polyimide laminate that provides chemical resistance and a good match for the thermal expansion coefficient of surface-mount technology parts. Boards were purchased to internal UI Quality Assurance (QA) standards for spaceflight hardware. All PWBs were baked and handled per standard UI QA procedures for spaceflight articles to remove absorbed moisture. All electrical assembly for the science payload was completed at the UI by a NASA certified technician. ICs with many leads were tacked and inspected by UI QA prior to final soldering. Wires needing to be lap soldered to PCBs were designed with a service loop to reduce stress. All aluminum components were chromate conversion coated at the UI Department of Physics and Astronomy Machine Shop. No conductive material was left floating to prevent potentially hazardous discharges and electric arcs. All fasteners were 4-40 stainless steel socket head cap screws fastened into two diameter tangless helicoil inserts. Instead of vented screws, blind holes were vented to prevent trapped volatile gasses or virtual leaks. All 4-40 fasteners were loaded with 0.56 $\mathrm{N} \cdot \mathrm{m}$ of torque with staking applied to the threads before permanent attachment. Large ICs, capacitors, inductors, and components were reinforced with lacing and staking material as necessary. For thermal and structural reinforcing, 3M 2216 was used. Arathane 5753 with 7% by volume filler was used for spot bonding and staking. Arathane 5750 conformal coating was applied to PCBs by brush coating and thickness was verified using a UV lamp.

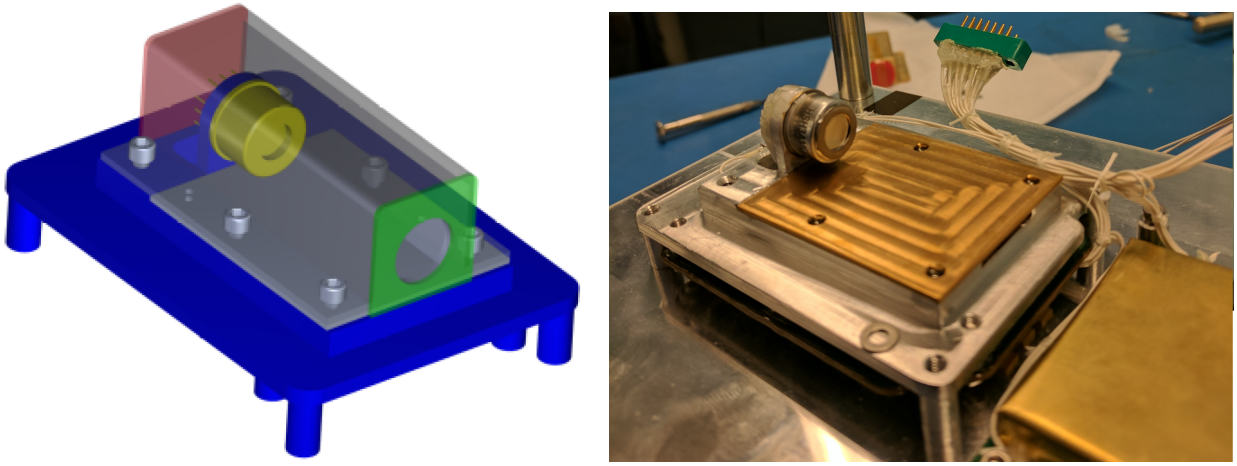

Fig 3 The detector assembly is at the core of the science payload. (Left) It contains an SDD X-ray detector (gold) attached to the baseplate tombstone (blue), a copper-tungsten passive shield comprised of a plate (gray) and a box (translucent gray, green, and red). The Amp-Chain PCB (not shown) is mounted on the underside of the baseplate to minimize path length for signal from the SDD prior to amplification. (Right) A picture of the detector assembly with the passive shielding box removed clearly showing the Amptek FAST SDD with the C1 window.

4 The Detector Assembly

The detector assembly (see Fig. 3) includes the X-ray detector, the passive radiation shield, and the front-end electronics responsible for shaping and amplifying the output signal from the detector into a useful waveform for reliable digitization. Each detector assembly is mounted at the rear of a detector compartment opposite the X-ray apertures.

4.1 X-ray Detectors

Several key factors guided the decision-making process for choosing a detector. First, the detector needed to be compatible with the CubeSat form factor, and it would also require the energy resolution necessary to complete the primary science objective ($\Delta E < 100$ eV). Any required filters or windows must allow for sufficient transmission of X-rays in the relevant energy band (0.4-2 keV). Furthermore, larger active areas allow for more X-rays to be measured for a given observation, improving performance. Another driving factor was the decision to use commercial off-the-shelf X-ray detectors to reduce development risk and the overall mission cost and design time. Finally,

the detector needs to accommodate the 100 square degree FOV necessary to observe the entire sky for at least 5,000 s for each pointing throughout mission lifetime.

Different methods have been successfully used to measure diffuse X-ray emission. Proportional counters lack the energy resolution required for *HaloSat*. Microcalorimeters provide excellent energy resolution but the required cryogenic cooling cannot currently be accomplished in the CubeSat 6U form factor. CMOS or CCD detectors have sufficiency energy resolution, but require optics that limit the FOV well below what is required for the mission.

The X-ray detectors used on *HaloSat* are SDDs, which measure the energy of an incoming X-ray from the amount of ionization it produces in high-purity silicon [8,9]. A series of concentric ring electrodes in the detector drift electron-hole pairs produced by the X-ray down a field gradient to a collection anode at the center. These solid-state detectors have sufficient energy resolution and active area to accomplish the science objectives of *HaloSat*. The SDDs used on *HaloSat* are FAST SDDs, or Ultra High Performance SDDs manufactured by Amptek, Inc (see Fig. 3). The FAST SDDs were chosen for their improved resolution and low energy transmission in comparison to other available SDDs. As an alternative, the Si-PIN X-ray detector from Amptek, Inc. was also considered, but the 6 mm^2 active area version would have reduced our collecting area, while the 25 mm^2 version does not have the energy resolution necessary for the mission.

Each SDD has an active area of 25 mm^2 collimated to 17 mm^2, and a thickness of 500 μm [10]. An embedded two-stage TEC cools the detector to an operating temperature inside a TO-8 hermetic package. A discrete HVPS negatively biases the SDD during operation. Similar detectors are used by NASA's Neutron star Interior Composition ExploreR (NICER) mission, and therefore detectors of this nature have undergone extensive environmental testing [11]. The effective area of each detector for 0.6 keV X-rays is 5.1 mm^2. The energy resolution was measured to be between

82 and 89 eV (FHWM) at the 0.677 keV F K line for the three detector units [6]. A sample spectrum showing a ground calibration observation can be seen in Fig. 4.

The transmission of X-rays in the relevant energy band for the Amptek FAST SDD was also an important factor. These FAST SDDs came in packages with C-*Series* X-ray windows and increased transmission down to 0.3 keV in comparison to other commonly used windows. There are two types of C-*Series* window. The C1 window has a 150 nm Si_3N_4 layer with a 250 nm thick grounded coating of aluminum, and the C2 window has a 40 nm Si_3N_4 layer with only a 30 nm thick grounded aluminum coating. For X-ray emission from elemental oxygen, the C2 window transmits 62%, while the C1 window transmits 29.4% [10]. However, the C1 window has effectively no transmission for IR/visible light, while the C2 window does not have IR/visible blocking. Both configurations for these detectors were tested in-lab and we found the C1 window version of the detector to have a stable detector energy resolution for a wider range of operating temperatures. *HaloSat* uses the C1 window version of the FAST SDDs. Using a conservative spacecraft power analysis, it was possible that *HaloSat* would not have sufficient power to operate all three detectors, therefore the higher detector operating temperature allowed by the C1 window provided significant margin increase for the power budget estimates. The higher temperature also increased the allowable spacecraft interface temperatures for payload operation. The IR/visible blocking for the C1 window also reduces the contamination from various sources including the moon and the atmosphere of the Earth.

The purpose of *HaloSat* is to observe the diffuse emission from the interstellar and circumgalactic medium, therefore the science payload was designed to have a large survey grasp, which is defined as the product of effective area and solid angle of the FOV. Increasing either the solid angle or the effective area also increases the collection of photons for a source with an angular ex-

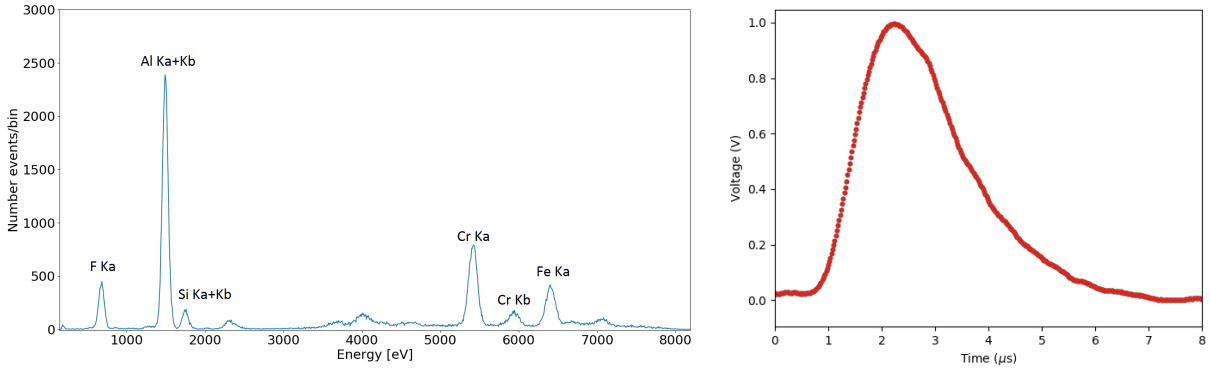

Fig 4 (Left) A calibration spectra from the science payload taken on the ground using an X-ray source fluorescing a piece of Teflon. Similar spectra were used to characterize the detectors using a number of characteristic lines over a range of energies. (Right) A sample X-ray pulse output from the detector assembly measured in the lab using an oscilloscope.

tent larger than the FOV. The grasp is therefore considered the figure of merit for diffuse emission studies. Although the effective area set by the detectors of *HaloSat* is low relative to other X-ray observatories, the large FOV and the high transmission at low energies make *HaloSat* a unique instrument capable of studying the halo over the entire sky in a relatively short mission life. The FOV of *HaloSat* was designed to be 100 square degrees for optimal observation of the halo. This FOV provided an appropriate sampling of targets over the entire sky to fit halo density distribution models, but also allowed a complete survey of the sky with few enough targets for greater than 5,000 s of observation each during the expected life of the mission.

4.2 Shielding

On a satellite in low-Earth orbit, increased count rates and even damage can result from the large flux of charged particles in the South Atlantic Anomaly (SAA). Due to the 51.6° orbital inclination, *HaloSat* frequently transits the SAA, and though events are not processed during these transits, shielding is still required. In addition to the SAA, local particles and cosmic rays can trigger events that contaminate the intended observation. Though the spacecraft and instrument housing

act as a shield to reduce radiation, each detector requires additional shielding to reduce background radiation from charged particle interactions.

The passive shield consists of two materials with different Z or atomic numbers, which is useful for blocking cascading radiation from incident particles and photons. To avoid the mechanical complexity of a traditional Z-graded shield, we chose to use a composite material with low and high Z components. Copper-tungsten (CuW) alloy was chosen as the shielding material. Tungsten has good shielding properties due to its high-Z, but is difficult to machine or cast. Using CuW increases machinability and adds a second lower-Z material to the shield, which provides many of the benefits of a Z-graded shield from a single material. The material used was a metal matrix composite comprised of 55% tungsten and 45% copper. The plate and the box are flashed with an inner layer of nickel (2.5 μm) and electroplated with an outer layer of gold (1.3 μm). Gold has no emission lines in the energy band of interest for *HaloSat* (0.4-2.0 keV), making it more desirable than copper, which has several emission lines in this band. Gold plating also prevents oxidation and resulting oxygen elemental lines that would contaminate the energy band of interest. While an electroless nickel finish would be less costly, nickel has lines similar in energy to oxygen. The properties of the shield (material, shape, and size) were designed in adherence to Orbital Debris Assessment Reports (ODAR) requirements.

The original design for the instrument used an active shield to reduce background by preventing processing of X-rays that coincided with high energy events fluorescing in the material that surrounded each detector. This shield, seen in Fig. 5 , consisted of two pieces of EJ-260 plastic scintillator made of a polyvinyl toluene (PVT) polymer base. The two pieces of scintillator were monitored using three silicone-window avalanche photo diodes (APD - S8664 from Hamamatsu Photonics). The APDs were attached to the scintillators using EpoTek 301 epoxy and cured in a

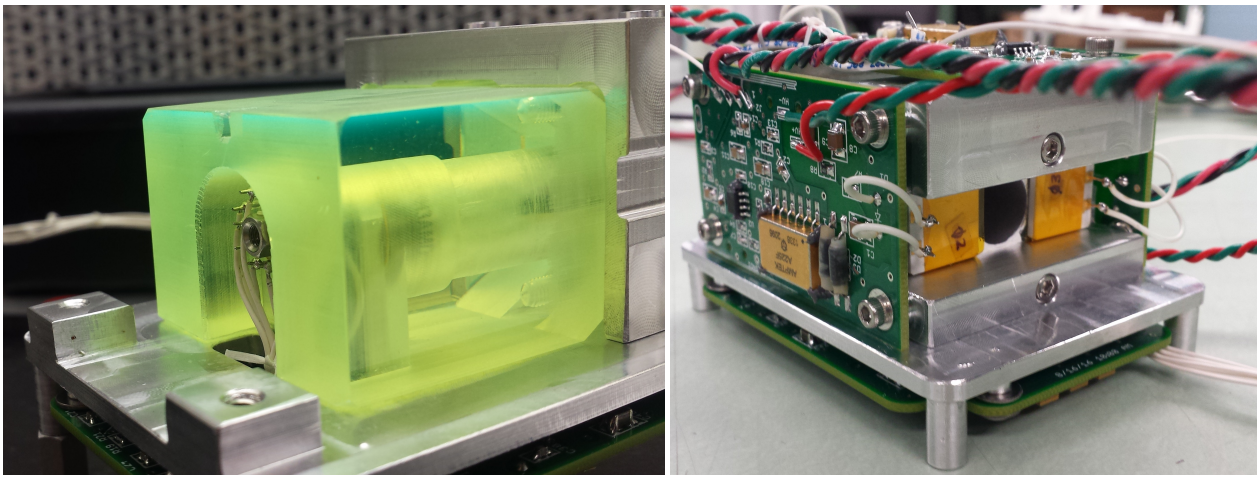

Fig 5 The original active shield designed and built for *HaloSat*. The scintillator (translucent yellow) would fluoresce from high energy interactions. This fluorescence was measured by three APDs and used to prevent events coincident with the fluorescence from triggering the event processing logic. (Left) The rear section of scintillator, which contained a single APD, is not installed, and the rear of the detector is visible showing the wire routing through the opening down to the front-end electronics. The scintillator is not yet painted. (Right) The scintillator, now painted white, with two APDs adhered to the front section with leads to the A225 PCBs. A polished hollow aluminum tube was inserted and epoxied inside the X-ray aperture of the scintillator.

nitrogen environment. A polished aluminum tube was inserted into the scintillator aperture opening and attached using EpoTek 301 epoxy. The unobstructed scintillator material was painted to prevent the fluorescent light from escaping before triggering an APD event. Each of the APDs had front-end electronics on a nearby A225 PCB. However, upon integration with the detector assembly and testing with a Co-60 source, it was found that the active shield did not provide effective background rejection. The low energy detection threshold for the active shield was measured to be 325 keV, which we believe was too high to provide effective rejection for the SDDs. Furthermore, a large fraction of events registered by the active shield did not have corresponding events in the SDD. By contrast, a purely passive shield could be implemented to reduce complexity and power consumption, and increase shielding. After examining simulations of the expected particle background and discussion with members of the NICER team, a passive shield was designed and implemented instead.

4.3 Pre-Amplification and Shaping Electronics

The SDD signal output from X-ray events requires amplification and shaping. To minimize noise pickup during amplification and shaping, the front-end electronics are located on the Amp-Chain PCB mounted close to the detector. The purpose of this PCB is to transform the charge pulse from the SDD into a shaped pulse with a peak voltage corresponding to the energy of the incident X-ray.

The pulse is shaped with a 1 μs shaping time using a high pass filter followed by a Sallen-Key band pass filter and another high pass filter. This pulse is amplified in several stages of the shaping filter chain to ensure that the Mn Kβ 6.49 keV transition line is visible for calibration and that the energy bins in the band of interest were appropriately sized. Pole-zero correction was fine-tuned on the engineering unit to reduce time for signal restoration to baseline following a pulse.

The output signal from the detector assembly contains positive amplitude X-ray pulses and bipolar reset pulses. The reset pulses occur when the charge built up on a capacitor in the detector is discharged. The reset pulses are distinguishable from X-ray event pulses by the negative voltage component on the output signal. An X-ray pulse from output from the detector assembly can be seen in Fig. 4.

5 Signal Processing Electronics

The output from the detector assembly is fed into the signal processing electronics to record X-ray events in a digital format. The output signal is fed into a peak detection and hold circuit, which consists of two MAX987 low-voltage comparators and an Amptek PH300 resettable peak-hold. The first comparator sets the voltage threshold for X-ray events, and the second sets a negative voltage threshold to signify a reset pulse. Each detector unit has individual threshold levels configured in software and initialized during the power-on sequence through a digital to analog converter

(DAC). The negative pulses are registered by inverting the output from the detector assembly and using a 1.0 V threshold. When a negative reset pulse is registered, the event is stored with a zero voltage pulse height. To avoid pile-up, until the output returns to baseline the instrument will not register additional events for 12 μs.

A threshold on the noninverted signal sets the limit above which the detector unit will register an X-ray event pulse. This threshold is set for each of the three detector units independently based on laboratory testing and corresponds to the noise floor of that detector unit. X-ray events are asynchronous, thus a synchronizer block is used to ensure the pulses are reliably interpreted. Pulses that exceed the threshold on the detector signal line begin the event capture state machine in the FPGA firmware. Following an event capture and after a delay, the PH300 holds the pulse height of the detector output while that height is digitized using a Linear Technology LTC2355IMSE-14 analog to digital converter (ADC) and recorded into memory with the pulse height amplitude and time of arrival (accurate to 0.05 s). Pulses above the maximum ADC bin are encoded with the maximum bin value of 16383, which is known as the overflow bin.

The pulse heights are stored in SRAM on the FPGA. The SRAM is configured as a FIFO to eliminate the need to read the event data immediately. Events are combined into groups of up to 30 and encoded into a data packet which is transmitted and stored on the spacecraft. To facilitate testing on the ground, it is possible to trigger an event from software and simulate pulses in a variety of different configurations. This allowed us to test the instrument and ensure the behavior operated as designed.

6 Interface and Control Electronics

The primary component of the interface and control electronics is a Microsemi A3PE1500-PQ208I FPGA programmed with a Systemyde Y90S System-on-Chip core located on the DPU PCB. The industrial grade of this FPGA was used as the operating temperature range for the commercial version did not cover the full range of expected payload temperatures. A 20.000 MHz Q-Tech QT83 crystal oscillator is also located on the DPU PCB, as well as a debugging interface for monitoring and programming the FPGA software. A JTAG interface is used to load the FPGA firmware from a host computer. The coding of DPU IDs appears in header for packets from each detector unit.

Each SDD requires a fixed negative bias between -110 and -200V to operate. For each of the three detector units a bias voltage of -135 V is produced by a dedicated HVPS with a set-point controllable in software. An AD5592 DAC on the Analog PCB sets the analog voltage value on the HVPS, which produces the output voltage of the HVPS. A monitor input on an AD5592 ADC on the Analog PCB measures the high-voltage output using a voltage divider. The set values for the DAC were determined in the lab for each HVPS to provide an output bias of -135 V and set in software. The HVPS was extensively tested and characterized over the range of ambient temperatures expected to experience on orbit.

The instrument must regulate the power supplied by the spacecraft into the various voltages required for the science payload to function. The spacecraft provides +5.0 V, +3.3 V, and electrical ground. The instrument uses EMI filtering circuits for spacecraft voltages to prevent AC line noise from entering the payload. The SDD requires +3.3 V, +2.0 V, and -3.0 V, several components require -5.0 V, and the FPGA requires 1.5 V.

All X-ray events must be understood in the context of the conditions of the spacecraft and the science payload at that moment. Hence, the instrument collects housekeeping data in a fixed format every 8 seconds. This includes monitor voltages, temperatures, set-points, command counters, and packet counters. The energy calibration of the instrument has a small dependence on temperature. The spacecraft does not maintain uniform temperature, therefore it is beneficial to use a number of temperature sensors. A 1N914 diode is adhered to each detector assembly baseplate and measures the ambient temperature experienced by the detector units. The DPU temperature is measured by a sensor on an Analog Devices ADT7311. Both the ADC and DAC on the Analog PCB also have temperature sensors.

To reduce dark current, the instrument operates with SDD detectors cooled to -30° C by a TEC located in the detector package. The SDDs need to operate at temperatures between -55° C to -20° C to achieve the energy resolution required by the primary science objective. The -30° C operating temperature kept our power consumption low and allowed the science payload to operate over the range of expected ambient temperatures. The TEC in the SDD TO-8 package has a cooling $\Delta \mathrm{T}_{\mathrm{max}}$ = 85 K, allowing for operation in ambient temperatures as warm as +55° C. Each SDD has a built-in 1N914 diode used to measure operating temperature. The ADU units for the temperature sensors are in 0.27° bin sizes. The on-orbit average operating temperatures are -30.1, -30.0, and -30.1° C for DPU 14, 54, and 38 respectively. The on-orbit RMS fluctuations in the SDD operating temperatures are 0.5, 0.4, and 0.2° C for DPU 14, 54, and 38 respectively.

A major component of the control electronics is the TEC controller, which maintains this operating temperature. Over the life of the mission, the spacecraft to instrument interface temperature varies during operation, and the SDDs must remain reliably cooled. The SDDs were extensively characterized at the operating temperature, and thus monitoring the temperature and keeping it

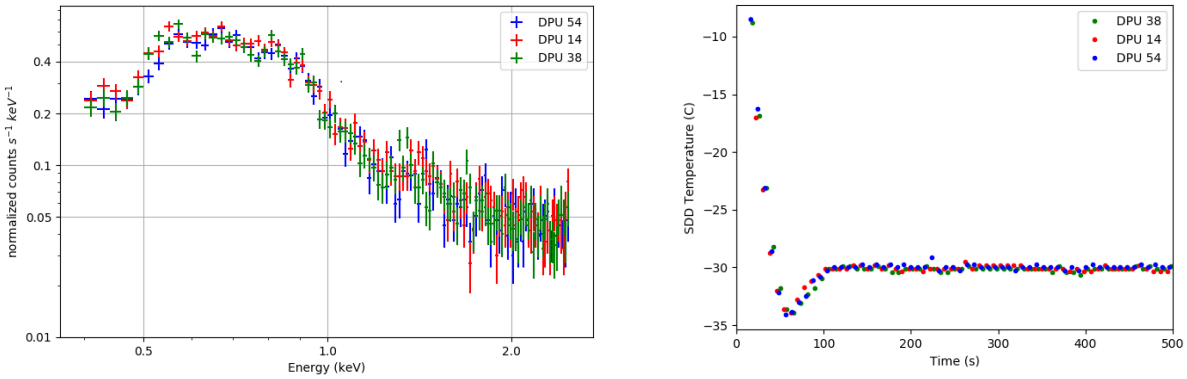

Fig 6 (Left) A sample spectrum taken in orbit of the diffuse emission from the North Polar Spur. (Right) A time series plot displaying the on-orbit SDD temperature for each of the three detector units following the power-on sequence. The detector is rapidly cooled with an overshoot before stabilizing to operating temperature.

stabilized are important tasks. The instrument uses a feedback loop to maintain a stable detector temperature by controlling the voltage applied to the TEC.

The TEC controller is a step-down voltage converter. The voltage produced by the TEC controller is set by a pulse-width modulated (PWM) signal for efficiency, with the PWM output switching between 3.3V and ground. The processor monitors the SDD temperature and adjusts the PWM control output voltage to achieve the set-point temperature of -30° C using a proportional-integral-derivative (PID) controller implemented in Y90S software. A PID loop is commonly used to maintain a control output at a desired set-point. The TEC controller adjusts the PWM signal duty cycle between 1% and 85%. The SDD temperature for an observation in orbit can be seen in Fig. 6.

Because the TEC is located directly under the detector chip the TEC controller could easily inject noise into the detector. To reduce potential switching noise in the detector output, the TEC control circuit output is heavily filtered by a high order LC lowpass filter. The circuit contains snubbers to dissipate high frequency energy. We opted to not add the hardware needed to use a discrete controller and instead implemented the control loop as a background process in the Y90S RTOS.

7 Housekeeping, Science, Command and Telemetry

The instrument has no non-volatile storage for housekeeping and science data. Therefore, all data accumulated during an observation must be transferred to the spacecraft before the instrument is switched off at the end of each observing sequence. The instrument DPU collects science and housekeeping data and constructs CCSDS compatible transfer packets, which are transmitted to the spacecraft data system for storage and eventual downlink.

There are three +3.3V CMOS communication lines between the spacecraft and the payload: one reset line, one data line, and one command line. There is a bi-directional Universal Asynchronous Receiver/Transmitter (UART) interface between the spacecraft and each detector unit for commands and telemetry. The spacecraft communicates commands and ancillary packets to each detector unit through one line. Each detector unit transmits packets to the spacecraft on its telemetry line. The interface is asynchronous and therefore no handshaking signals are required. The baud rate for this interface is 57.6 kbps.

Spacecraft time and attitude information is sent to the instrument as ancillary data every 2 seconds and included in the instrument telemetry. This simplifies ground data processing because no spacecraft packets need to be separately processed and time aligned with the instrument data to determine pointing information. This ancillary information includes the current time, the position coordinates in Earth-Centered-Earth-Fixed (ECEF), the velocity in ECEF, and the 3D rotation in a quaternion (ECI J2000). This information is used on the ground to calculate satellite latitude, satellite longitude, altitude, and boresight coordinates at a specific time.

The instrument generates event data in the form of a pulse height amplitude and an instrument time. These events are combined into groups of up to 30 in packets. The internal instrument time

stamps are stored alongside ancillary packets containing the current GPS time from the spacecraft, which is used on the ground to calculate times for the events. The current GPS time is reconstructable to UTC to within an accuracy of 0.5 seconds and the transmission of the GPS time occurs within 0.1 seconds of the time indicated in the ancillary information message. Each detector unit formats science data and housekeeping information into transport frames with header information that identifies the detector. On the ground, the data are processed and formatted into spectra as in Fig. 6.

The DPU software is based on a custom Real Time Operating System (RTOS) first developed for the radio and plasma wave science instrument onboard the Cassini mission to Saturn [12]. The software was subsequently upgraded for the Waves instrument onboard the Juno mission to Jupiter [13]. The RTOS was ported to the Y90S processor under a grant from the Iowa Space Grant Consortium and is referred to as the FLEXI system. The RTOS is preemptive multitasking and has significant reuse of code from Waves for handling CCSDS output packets, instrument commanding, and timing.

Commands can be sent individually to any of the three detector units or to all three simultaneously. The first section of each command is a BCT sync pattern. The following section is a FLEXI command header containing the DPU serial number and a command length. Next is the individual FLEXI command specifying the type of command and the length.

A cyclic redundancy check (CRC) is located in the final 16 bits of all telemetry and commands. This CRC is in accordance with the CCSDS CRC-16. These specifications use the generator polynomial $x^{16} + x^{12} + x^5 + 1$, which is commonly known as CCITT-16. It has a Hamming distance, or the minimum number of bit flips that can create an undetectable error, of 4 at dataword length 1 to 32751 [14] and is well-suited for detection of burst errors shorter than 16 bits. The seed

value is zero.

8 Conclusion

At the time of this writing, *HaloSat* has been operating nominally for over one year on-orbit and has observed all of its all-sky fields. The environment of space can be volatile, but adherence to best practices and making informed design choices can drastically increase the reliability of CubeSats and their payloads. While the UI team has members with considerable experience in building hardware for operation in space, the team has minimal previous experience with CubeSats. Harnessing the expertise of both NASA and the commercial industry can help bolster reliability and allow a team that is inexperienced with the CubeSat platform to launch a successful mission. Direct guidance and support provided by NASA helped *HaloSat* adhere to best practices and ensure the success of the mission. Collaboration with BCT for the construction of a commercial bus avoided several barriers to entry such as attitude determination and control systems. An EDU unit provided by BCT allowed the two teams to test the interface between the spacecraft and the instrument before integration and make changes to software as needed, which was likely a key to our seamless integration. BCT also serves as the MOC for *HaloSat*, and while some CubeSat teams will choose to conduct mission operations, working with a company such as BCT is a viable alternative.

As part of a lower cost mission with a specified concept of operation, the instrument onboard *HaloSat* could be fine-tuned for a dedicated purpose in both design and observing strategy. By maximizing the survey efficiency and grasp of the instrument, our CubeSat can be competitive with major space observatories and provide value in a specific area. The rapid development, integration, and launch schedule of 2.5 years for CubeSats is sure to garner more interest in the field of astrophysics as both a test bed for new technology as well as a platform for focused missions.

HaloSat may be one of the first astrophysics CubeSats, but it will not be the last.

Acknowledgments

This research was supported by NASA grant NNX15AU57G. We would like to acknowledge our NASA mission systems engineer Luis Santos for his invaluable guidance and expertise throughout the design and construction, Tracy Behrens for her work assembling the *HaloSat* electronics, Rich Dvorsky for mechanical and polymerics advice and guidance, Brian Busch, Larry Detweiler, and Matt Miller for their work in the machine shop, Tim Cameron for building the HVPS, Kayla Racinowski for helping with polymerics and inductors, Jeff Dolan for assistance with connectors and electronics, Jim Phillips for guidance with inductor cores, Jesse Haworth for designing the *HaloSat* logo and for his work on the HVPS, Riley Wearmouth for early mechanical designs, John Hudeck for his assistance with vibration testing, Systemyde international for supplying the Y90S, Brian Mokrzycki for providing the Verliog for the FPGAs, Steve Schneider, Doug Laczkowski, Chris Esser, Karl Hansen, Nancy Gaytan, and the BCT team for their work on the spacecraft bus and acting as the MOC, and the WFF UHF Ground Station Team for their support of *HaloSat* in orbit.

References

1 R. Hevner, W. Holemans, J. Puig-Suari, *et al.*, "An advanced standard for cubesats," (2011).

2 J. Puig-Suari, C. Turner, and R. Twiggs, "Cubesat: the development and launch support infrastructure for eighteen different satellite customers on one launch," (2001).

3 M. Swartwout, "Cubesat database," https://sites.google.com/a/slu.edu/swartwout/home/cubesat-database (accessed 08/15/2019). (2019).

4 P. Kaaret, A. Zajczyk, D. LaRocca, *et al.*, "First results from halosat-a cubesat to study the hot galactic halo," in *AIAA/USU Conference on Small Satellites, Year in Review 1, SSC19-TSIII-04*, https://digitalcommons.usu.edu/smallsat/2019/all2019/277/ (2019).

5 K. Kuntz, "Solar wind charge exchange: an astrophysical nuisance," *The Astronomy and Astrophysics Review* **27**(1), 1 (2019).

6 A. Zajczyk, P. Kaaret, D. Kirchner, *et al.*, "Halosat: A search for missing baryons with a cubesat," in *AIAA/USU Conference on Small Satellites, Upcoming Missions, SSC18-WKIX-01*, https://digitalcommons.usu.edu/smallsat/2018/all2018/471/ (2018).

7 A. Poghosyan and A. Golkar, "Cubesat evolution: Analyzing cubesat capabilities for conducting science missions," *Progress in Aerospace Sciences* **88**, 59–83 (2017).

8 E. Gatti and P. Rehak, "Semiconductor drift chamber—an application of a novel charge transport scheme," *Nuclear Instruments and Methods in Physics Research* **225**(3), 608–614 (1984).

9 C. Gauthier, J. Goulon, E. Moguiline, *et al.*, "A high-resolution silicon drift chamber for x-ray spectroscopy," *Nuclear Instruments and Methods in Physics Research Section A: Accelerators, Spectrometers, Detectors and Associated Equipment* **349**(1), 258–262 (1994).

10 Amptek, "Fast sdd ultra high performance silicon drift detector," https://www.amptek.com/products/sdd-x-ray-detectors-for-xrf-eds/fast-sdd-silicon-drift-detector (accessed 08/13/2019). (2019).

11 K. C. Gendreau, Z. Arzoumanian, P. W. Adkins, *et al.*, "The neutron star interior composition explorer (nicer): design and development," in *Space Telescopes and Instrumentation 2016:*

Ultraviolet to Gamma Ray, **9905**, 99051H, International Society for Optics and Photonics (2016).

12 D. A. Gurnett, W. S. Kurth, D. Kirchner, *et al.*, "The cassini radio and plasma wave investigation," in *The Cassini-Huygens Mission*, 395–463, Springer (2004).

13 W. Kurth, G. Hospodarsky, D. Kirchner, *et al.*, "The juno waves investigation," *Space Science Reviews* **213**(1-4), 347–392 (2017).

14 P. Koopman, "Crc polynomial zoo," https://users.ece.cmu.edu/koopman/crc/crc16.html (accessed 08/14/2019). (2018).

Daniel LaRocca is a graduate student at the University of Iowa. He received his BA in physics from Illinois Wesleyan University in 2013, and is currently pursuing a PhD degree in Physics and Astronomy. He was a member of the team that built the *HaloSat* science payload and worked with BCT to integrate the science payload with the spacecraft. He is in charge of science operations scheduling for the mission. His current research interests pertain to diffuse X-ray emission and he is particularly interested in the North Polar Spur.

List of Figures

List of Tables